

COSMIC RAY DIFFUSION FRONTS IN THE VIRGO CLUSTER

WILLIAM G. MATHEWS¹ AND FULAI GUO¹

Draft version October 26, 2018

ABSTRACT

The pair of large radio lobes in the Virgo cluster, each about 23 kpc in radius, have curiously sharp outer edges where the radio-synchrotron continuum flux declines abruptly. However, just adjacent to this sharp transition, the radio flux increases. This radio limb-brightening is observed over at least half of the perimeter of both lobes. We describe slowly propagating steady state diffusion fronts that explain these counterintuitive features. Because of the natural buoyancy of radio lobes, the magnetic field is largely tangent to the lobe boundary, an alignment that polarizes the radio emission and dramatically reduces the diffusion coefficient of relativistic electrons. As cosmic ray electrons diffuse slowly into the cluster gas, the local magnetic field and gas density are reduced as gas flows back toward the radio lobe. Radio emission peaks can occur because the synchrotron emissivity increases with magnetic field and then decreases with the density of non-thermal electrons. A detailed comparison of steady diffusion fronts with quantitative radio observations may reveal information about the spatial variation of magnetic fields and the diffusion coefficient of relativistic electrons. On larger scales, some reduction of the gas density inside the Virgo lobes due to cosmic ray pressure must occur and may be measurable. Such X-ray observations could reveal important information about the presence of otherwise unobservable non-thermal components such as relativistic electrons of low energy or proton cosmic rays.

Subject headings: cosmic rays; diffusion; radio continuum; galaxies: clusters; galaxies: clusters: individual Virgo; magnetic fields

1. INTRODUCTION

Several nearby galaxy clusters contain extended non-thermal radio lobes that appear to be unrelated to currently visible X-ray cavities. For example, the iconic image of the Virgo cluster at 90 cm (325 MHz) from Owen, Eilek & Kassim (2000), shown in Figure 1, features two large opposing quasi-circular radio lobes. (The famous 2 kpc radio jet in M87 is over-exposed in the central dark region.) In Mathews & Brighenti (2008a) we proposed that the Virgo radio lobes were formed by relativistic electrons that diffused through the walls of X-ray cavities that have long-since buoyantly risen and disappeared from view. This conjecture seemed attractive because a 25-kpc long radial thermal X-ray filament (Young, Wilson & Mundell 2002; Forman, et al. 2005; Werner, N. et al. 2010; Million et al. 2010) passes in projection right through the center of the southern Virgo lobe, suggesting that both were formed in the same X-ray cavity event. Moreover, the radio-synchrotron spectral age of the oldest and most distant electrons in the Virgo lobes, $t_{sync} \approx 10^8$ yrs, matches the dynamical age of the post-cavity filament as computed by Mathews & Brighenti (2008a) who suggested that the radio-synchrotron electrons currently filling the southern lobe may have diffused through the walls of the same filament-forming X-ray cavity. Cosmic ray electrons freely diffusing isotropically from the center of the southern lobe of radius $r_{lobe} \approx 23$ kpc suggests a diffusion coefficient $\kappa \approx r_{lobe}^2/t_{sync} \approx 10^{30}$ cm² s⁻¹. But a potential difficulty with a simultaneous origin for the thermal X-ray

filament and southern Virgo lobe is the absence of a corresponding radial thermal filament in the northern lobe.

In addition, we now suspect that the Virgo radio lobes have a more complex evolution resulting from a multitude of active galactic nucleus (AGN) outbursts that continuously resupply cosmic ray electrons to the lobes, a point of view also suggested by Owen, Eilek & Kassim. The 8-shaped Virgo lobes may represent an approximately bipolar energy ejection pattern from the central black hole in M87. AGN jet and cavity activity in Virgo (as in Perseus and many other clusters) rarely occurs along a fixed bipolar axis as defined for example by an unchanging black hole spin, but jet energy may be distributed in directions near such an axis. As a consequence, the Virgo lobes may expand much slower and be older than implied by free cosmic ray diffusion.

With this in mind, we draw attention in Figure 1 to the sharp transition at the outer boundary of the Virgo radio lobes where the radio flux abruptly decreases, completely unlike the smooth gaussian transition expected for free diffusion with $\kappa \sim 10^{30}$ cm² s⁻¹. Owen, Eilek and Kassim (2000) emphasize that the sudden decrease in radio flux at the lobe boundary is real, not an artifact of image-processing software. Another curious widespread feature just at this lobe-cluster gas transition are the bright synchrotron-emitting rims visible in Figure 1 immediately adjacent to the sudden sharp drop to zero radio flux. According to Owen, Eilek and Kassim, this counterintuitive radio limb-brightening is present in over half of the perimeter of both lobes.

In the following discussion we propose that the bright radio rims can be understood if the diffusion coefficient of synchrotron-emitting electrons decreases sharply near the lobe-cluster gas boundaries.

¹ University of California Observatories/Lick Observatory, Department of Astronomy and Astrophysics, University of California, Santa Cruz, CA 95064 mathews@ucolick.org

2. PLANE PARALLEL STEADY DIFFUSION FRONT

We assume that cosmic rays (relativistic electrons and/or protons) in the radio lobes are coupled to the gas by means of a magnetic field frozen into the gas through which cosmic rays may diffuse. While the magnetic field allows cosmic ray pressure gradients to act on the cluster gas, the small magnetic energy density is dynamically negligible. Magnetic fields of strength 0.3–10 μG are ubiquitous in cluster gas (Govoni & Feretti 2004). In general the magnetic field decreases with cluster radius and decreasing gas density. An approximate powerlaw relation $B \propto n_e^s$ with $0.4 \lesssim s \lesssim 0.7$ in the Coma cluster gas has been established from Faraday depolarization observations of cluster galaxies (Bonafede et al. 2010). However, fields with energy densities $B^2/8\pi = 6 \times 10^{-13}(B/4\mu\text{G})^2 \text{ erg cm}^{-3}$ cannot significantly influence the dynamics of local cluster gas with a much larger thermal energy density $3P/2 = 5 \times 10^{-11}(n_e/0.01 \text{ cm}^{-2})(T/\text{keV}) \text{ erg cm}^{-3}$, and $B^2/8\pi \ll 3P/2$ probably holds at every radius in the cluster gas. In view of this, magnetic fields need not explicitly appear in the dynamical equations:

$$\frac{\partial \rho}{\partial t} + \nabla \cdot \rho \mathbf{u} = 0 \quad (1)$$

$$\rho \left(\frac{\partial \mathbf{u}}{\partial t} + (\mathbf{u} \cdot \nabla) \mathbf{u} \right) = -\nabla(P + P_c) \quad (2)$$

$$\frac{\partial e}{\partial t} + \nabla \cdot \mathbf{u} e = -P(\nabla \cdot \mathbf{u}) \quad (3)$$

$$\frac{\partial e_c}{\partial t} + \nabla \cdot \mathbf{u} e_c = -P_c(\nabla \cdot \mathbf{u}) + \nabla \cdot (\kappa \nabla e_c) \quad (4)$$

where $e = P/(\gamma - 1) = 3P/2$ and $e_c = P_c/(\gamma_c - 1) = 3P_c$ are the energy density-pressure relations for gas and cosmic rays respectively and κ is the diffusivity of cosmic rays. Weak magnetic fields evolve passively, advecting with the gas. These equations are discussed further in Mathews & Brighenti (2008a,b).

Recognizing the relatively short time for gas to flow past the radio lobe boundary, we do not consider the energy lost by thermal or non-thermal radiation as gas flows through the boundary rims. The time required for gas flowing at velocity $u \approx 20 \text{ km s}^{-1}$ to cross the bright radio rims of thickness $\Delta x \lesssim 0.6 \text{ kpc}$ is $t_{flow} = \Delta x/u \lesssim 3 \times 10^7 \text{ yrs}$. However, the radiative cooling time in the ambient gas near the radio lobes ($\rho \approx 2.5 \times 10^{-26} \text{ g cm}^{-3}$, $T \approx 2.5 \times 10^7 \text{ K}$) is much longer, $t_{cool} \approx 5m_p kT/\Lambda(T)\mu\rho \approx 2.7 \times 10^9 \text{ yrs}$, where $\Lambda(T)$ is the usual coefficient for optically thin thermal emission. Furthermore, the calculation we consider is embedded in the gravitationally supported hot gas atmosphere in a galaxy cluster where local cooling after the loss of energy by radiative emission does not occur. Any decrease in the local gas temperature due to radiative losses is rapidly reversed by a global compression and gas inflow that maintains the virial temperature and pressure required to support the entire atmosphere. Moreover, no thermal jump associated with the Virgo radio lobe boundaries has been observed in detailed X-ray observations (Million et al. 2010). Non-thermal electrons of energy $\gamma = E/m_e c^2 \approx (2\pi m_e c^2/3B\lambda)^{1/2} \approx 6 \times 10^3$ radiating in

a $3\mu\text{G}$ field produce synchrotron emission at $\lambda = 90 \text{ cm}$ as in Figure 1. The synchrotron lifetime for these electrons, $t_{sync} = \gamma/\dot{\gamma} = (3m_e c/4\sigma_T)(4\pi/B^2\gamma) \approx 1.1 \times 10^8 \text{ yrs}$, also exceeds t_{flow} . However, the local synchrotron lifetime is not particularly relevant for our diffusion front calculation where new cosmic ray electrons are continuously provided by diffusion from the adjacent radio lobe. But we do assume that the synchrotron radio spectral index α , appropriate for a power law distribution of electron energies, remains constant across the diffusion front. Finally, since the flow time across the diffusion front at the lobe boundary is almost certainly less than the dynamical age of the lobe itself, the diffusion front structure is approximately in steady state during times $\sim t_{flow}$.

For simplicity, and consistency with current Virgo X-ray observations, we consider the cluster gas to be isothermal in the vicinity of the radio lobe-cluster gas boundary, with pressure, $P = \rho c_s^2$, depending only on the isothermal sound speed which replaces equation (3). The cosmic ray energy density e_c is integrated over the relativistic energy or momentum distribution, $e_c \propto \int EN(E)dE \propto \int p^4 f(p)(1+p^2)^{-1/2} dp$ and may refer to electrons and/or protons.

For steady-state, one-dimensional, plane-parallel, isothermal flow near the lobe-gas boundary these equations reduce to:

$$\frac{d(\rho u)}{dx} = 0 \quad (5)$$

$$\frac{d}{dx}[\rho u^2 + P + P_c] = 0 \quad (6)$$

$$\frac{d(e_c u)}{dx} + P_c \frac{du}{dx} - \frac{d}{dx} \left(\kappa \frac{de_c}{dx} \right) = 0. \quad (7)$$

Equations (5) and (6) are directly integrable

$$\rho u = A \quad \text{and} \quad [\rho(u^2 + c_s^2) + P_c] = B \quad (8)$$

where $u < 0$ and $A < 0$. For a steady diffusion front propagating in the positive x direction, in our calculation, performed in the rest frame of the front, the gas flows in the negative x direction from the cluster gas toward the lobe – the direction of increasing x is shown with the small arrow in Figure 1. Eliminating ρ between equations (8) results in a quadratic for u

$$u^2 + u \frac{1}{A} \left(\frac{e_c}{3} - B \right) + c_s^2 = 0 \quad (9)$$

for which the desired solution is

$$u = \frac{1}{2} \left\{ -\frac{1}{A} \left(\frac{e_c}{3} - B \right) + \left[\frac{1}{A^2} \left(\frac{e_c}{3} - B \right)^2 - 4c_s^2 \right]^{1/2} \right\}. \quad (10)$$

By differentiating equation (9)

$$\frac{du}{dx} = -\frac{u}{3b} \frac{de_c}{dx} \quad \text{where} \quad b = 2Au + [(e_c/3) - B], \quad (11)$$

equation (7) can be written as

$$u \frac{de_c}{dx} - \frac{4e_c u}{9b} \frac{de_c}{dx} - \frac{d}{dx} \left(\kappa \frac{de_c}{dx} \right) = 0. \quad (12)$$

The x -dependence of κ can be subsumed into a new independent variable

$$\xi = \int \frac{dx}{\kappa} \quad (13)$$

by multiplying each term of equation (12) by κ ,

$$u \frac{de_c}{d\xi} - \frac{4e_c u}{9b} \frac{de_c}{d\xi} - \frac{d^2 e_c}{d\xi^2} = 0 \quad (14)$$

which can be solved as a pair of first order equations for dependent variables $\phi \equiv de_c/d\xi$ and e_c ,

$$\frac{d\phi}{d\xi} = u\phi \left(1 - \frac{4e_c}{9b}\right) \quad \frac{de_c}{d\xi} = \phi. \quad (15)$$

Once $e_c(\xi)$ is known, $u(\xi)$ follows from (10), and the density $\rho(\xi) = A/u(\xi)$.

Solutions of these equations describe a steady state 1D diffusion front representing the dynamical encounter between cluster gas containing cosmic rays inside the radio lobe on the small- ξ side and approaching external cluster gas on the large- ξ side containing no cosmic rays. The gas pressure must increase in the ξ -direction by $P_c = e_c/3$ to keep the total pressure $P_t \approx P + P_c$ nearly uniform in subsonic flow, $u \ll c_s$. Since no X-ray cavities are known to be associated with the Virgo radio lobes, it is likely that the cluster gas pressure contributes substantially within the lobes, i.e. the Virgo lobes are partial X-ray cavities, only modestly depleted of cluster gas. The plane-parallel equations are valid within a distance from the lobe boundary that is small compared to the 23 kpc radius of the Virgo lobes. The solution profiles in $\xi - e_c(\xi)$, $\rho(\xi)$, $u(\xi)$, $P(\xi)$, etc. – are universal, valid for any assumed spatial variation of the cosmic ray diffusion coefficient $\kappa(x)$.

Without loss of generality, we assume that $\xi = 0$ at some arbitrary position $x = 0$ within the Virgo radio lobe where gas with temperature $T_0 = 2.5 \times 10^7$ K and density $\rho_0 = 2.5 \times 10^{-26}$ gm cm $^{-3}$ ($n_{e,0} = 0.0129$ cm $^{-3}$) flows away from the front with velocity $u_0 < 0$ and with a cosmic ray to gas pressure ratio $(P_c/P)_0$ from which $e_{c,0}$ can be found. Our integration of equations (15) begins inside the radio lobe at $\xi = 0$, where flow variables have subscript “0”, and proceeds upstream toward the diffusion front at larger ξ . The initial gas pressure $P_0 = \rho_0 c_s^2$ cannot be changed much since the density and temperature (sound speed $c_s = 580$ km s $^{-1}$) are chosen to approximately match those observed in the Virgo cluster near the lobes (Ghizzardi, et al. 2004). The velocity u_0 , cosmic ray energy density $e_{c,0}$ and its slope $\phi_0 = (de_c/d\xi)_0$ at $\xi = 0$ can be changed to alter the morphology of the front. The numerical integration of equations (15) proceeds from $\xi = 0$ toward positive ξ until e_c becomes very small.

We consider two representative subsonic flow velocities u_0 at $\xi = 0$. The first is a characteristic velocity for old Virgo lobes, $u_0 \approx -23$ kpc/10 9 yr ≈ -20 km s $^{-1}$ and the second is somewhat larger, $u_0 = -100$ km s $^{-1}$. The upper three panels of Figure 2 show these two solutions as functions of the universal κ -independent variable ξ . Notice that as e_c approaches zero at some finite $\xi = \xi_1$ at the leading edge of the diffusion front, the gas velocity is asymptotically finite and negative as cluster gas enters

the front; the second term in equation (14) also vanishes at ξ_1 , indicating that diffusion at the leading edge of the front is balanced by advection downstream. We find $\xi_1 = 2.65 \times 10^{-8}$ and 3.13×10^{-8} s cm $^{-1}$ for $u_0 = -20$ and -100 km s $^{-1}$ respectively.

For the limiting case of a static lobe-cluster gas front where $u \rightarrow 0$, the total pressure $P_t = P + P_c$ is everywhere exactly uniform and equation (14) becomes simply

$$\frac{d}{d\xi} \left(\frac{de_c}{d\xi} \right) = 0. \quad (16)$$

The solution in this case is linear $e_c(\xi) = e_{c,0} + \phi_0 \xi$ with uniform slope $de_c/d\xi = \phi_0 < 0$. The gas pressure $P(\xi) = P_t - e_c/3$ and density $\rho(\xi) = [P_t - (e_c/3)]/c_s^2$ profiles are also linear. Since the flow velocities we consider $|u_0|$ are much smaller than the sound speed c_s , the solutions plotted in Figure 2 resemble those of static fronts. These idealized static solutions are not solutions of the time-dependent diffusion equation and represent a mathematical limit that may not be physically relevant.

Steady state cosmic ray diffusion fronts occur only in a gasdynamical environment. In free isotropic cosmic ray diffusion in a stationary gas ($\mathbf{u} = 0$) solutions of the diffusion equation $\partial e_c / \partial t = \nabla \cdot (\kappa \nabla e_c)$ depend only on a similarity variable $\zeta = r^2/t$ and have no steady state solution. However in Figure 2 we see that steady solutions are indeed possible in a fluid environment.

2.1. Radio Synchrotron Emissivity

Computation of the synchrotron emission at a fixed radio frequency in the diffusion front requires knowledge of the density of relativistic electrons and the magnetic field strength and orientation. Radio polarization observations of Virgo at 2.8 cm by Rottmann et al. (1996) shown in Figure 3 reveal a remarkably high degree of linear polarization ($\gtrsim 70\%$), particularly near the outer edges of the lobes where the field direction is highly ordered. Field vectors plotted in Figure 3 indicate that the direction of the magnetic field is tangent to the boundary of both lobes over most of the lobe perimeter. This is consistent with the relative compression in Figure 2 near the lobe-cluster gas boundary at $\xi = \xi_1$. In our calculation the magnetic field evolves passively with the gas but does not have sufficient energy density to influence the flow parameters. In a one-dimensional flow with approximately perpendicular field alignment, magnetic flux is conserved if $B \propto \rho$.

For a power law distribution of relativistic electron energies, $N(E)dE = K E^{-p} dE$ with $p > 2$ the total energy density of cosmic ray electrons is

$$e_c = \int_{E_{min}}^{E_{max}} EN(E)dE = \frac{K}{(p-2)} (E_{min}^{2-p} - E_{max}^{2-p}) \quad (17)$$

$$\approx \frac{K}{(p-2)} E_{min}^{2-p}$$

and therefore $K \propto e_c E_{min}^{p-2}$. As the magnetic field slowly varies across the diffusion front, the relativistic adiabatic invariance of the electron magnetic moment requires that $\beta_{\perp} \gamma \propto B^{1/2}$ (Sturrock 1994) so $E_{min} \propto B^{1/2}$ and $K \propto e_c B^{\frac{1}{2}(p-2)}$. For electrons with intermediate energies, $E_{min} \ll E \ll E_{max}$, the synchrotron emissivity

from the electron distribution is

$$j_\nu \propto KB(\nu/B)^{-\alpha} \quad (18)$$

(Longair, 1994) where we assume $p = 2.5$ and $\alpha = (p - 1)/2 = 0.75$. Combining these dependencies, the radio synchrotron emissivity observed at the same frequency over the whole profile should vary with e_c and ρ as

$$j_\nu \propto e_c B^{\frac{1}{2}(p-2)} \cdot B \cdot B^{\frac{1}{2}(p-1)} \propto e_c \rho^\beta \quad (19)$$

where

$$\beta = \frac{1}{2}(2p - 1) = \frac{1}{2}(4\alpha + 1) \quad (20)$$

so $\beta = 2$ when $p = 2.5$. Owen, Eilek & Kassim (2000) suggest a mean index $\alpha \approx 1.0$ for Virgo for which $\beta = 2.5$. The index α may be even steeper near the lobe boundaries or vary with x , but current observations do not warrant such refinements.

What is the condition that the emissivity $j_\nu \propto e_c \rho^\beta$ (where $\beta \approx 2$) has a limb-brightened maximum at some ξ in the diffusion front? Since e_c always tends to zero as $\xi \rightarrow \xi_1$ near the leading edge of the diffusion front, a maximum is guaranteed if the emissivity increases with ξ at $\xi = 0$, i.e.

$$\frac{1}{j_\nu} \frac{dj_\nu}{d\xi} = \frac{1}{e_c} \frac{de_c}{d\xi} + \beta \frac{1}{\rho} \frac{d\rho}{d\xi} > 0 \quad (21)$$

at $\xi = 0$. Using $A = \rho u$ and equation (11), the density derivative in the second term can be written

$$\frac{1}{\rho} \frac{d\rho}{d\xi} = -\frac{1}{u} \frac{du}{d\xi} = \frac{1}{3b} \frac{de_c}{d\xi}. \quad (22)$$

The condition for a maximum in j_ν is then

$$\frac{\phi}{e_c} + \frac{\beta\phi}{3b} = \frac{\phi}{e_c} \left[1 + \beta \frac{P_c}{\rho u^2 - \rho c_s^2} \right] > 0 \quad (23)$$

at $\xi = 0$. Since $\phi_0 = (de_c/d\xi)_0$ is always negative, the quantity in brackets must also be negative. Furthermore, we expect diffusion fronts to be highly subsonic, $u^2 \ll c_s^2$, so the condition for a synchrotron emission maximum in the diffusion front is

$$\frac{P_c}{P} > \frac{1}{\beta} = \frac{2}{4\alpha + 1} \quad \text{or} \quad \frac{P_c}{P + P_c} > \frac{1}{1 + \beta} = \frac{2}{4\alpha + 3} \quad (24)$$

inside the lobe at $\xi = 0$. Normalized emissivity profiles $j_\nu(\xi)/j_\nu(0)$ with $\beta = 2$ are plotted in the lowest panel of Figure 2 for the two chosen values of u_0 and for $(P_c/P)_0 = 1$ which produces the desired maximum for radio limb brightening.

The spatial variation of e_c and other parameters with the true spatial coordinate x can be found for any assumed $\kappa(x)$ by integrating $dx/d\xi = \kappa$ to determine $x = x(\xi)$. If κ is constant, then ξ in the solutions in Figure 2 can simply be replaced with x/κ .

2.2. Diffusion Fronts in Physical Space

From any solution in variable ξ like those in Figure 2 an infinite variety of solutions in physical space $x(\xi)$ can be found by choosing various functions $\kappa(x) = dx/d\xi$. In particular, very sharply decreasing profiles $e_c(x)$ and $j_\nu(x)$ can be generated even when $e_c(\xi)$ and $j_\nu(\xi)$ are

very slowly varying. By this means, $x(\xi)$ could be chosen to match the limb-brightened $j_\nu(x)$ and radio flux observed at the edge of the Virgo lobes.

Since the diffusion coefficient κ must be positive, the spatial coordinate x must be an increasing function of ξ with positive slope $\kappa = dx/d\xi > 0$. We consider two simple examples for $x = x(\xi)$ normalized so that $x(\xi = 0) = 0$:

$$\text{Case I:} \quad \frac{x}{x_0} = (1 - e^{-\xi/\xi_0}) \quad (25)$$

$$\kappa = \frac{dx}{d\xi} = \frac{x_0}{\xi_0} e^{-\xi/\xi_0} = \frac{x_0}{\xi_0} \left[1 - \frac{x}{x_0} \right] \quad (26)$$

and

$$\text{Case II:} \quad \frac{x}{x_0} = \tanh\left(\frac{\xi}{\xi_0}\right) \quad (27)$$

$$\kappa = \frac{dx}{d\xi} = \frac{x_0}{\xi_0} \cosh^{-2}\left(\frac{\xi}{\xi_0}\right) = \frac{x_0}{\xi_0} \left[1 - \left(\frac{x}{x_0}\right)^2 \right]. \quad (28)$$

For both cases the physical scale of the front extends from $x = 0$ to $x = x_0$ where κ becomes zero. The parameter ξ_0 characterizes the rate of distortion of the ξ -profiles into x -profiles with smaller values of ξ_0 concentrating the x -profiles closer to $x = x_0$.

Figure 4 shows the variation of $\kappa(x)$ and $j_\nu(x)/j_\nu(0)$ for both Case I and II with $x_0 = 1$ kpc for three values of ξ_0 , all for the $u_0 = -20$ km s⁻¹ solution plotted in Figure 2. Figure 5 shows the spatial variation of the flow variables on the radio lobe side of the diffusion front, $\rho(x)$, $u(x)$, $B(x)$, $P_c(x)$ and $P(x)$ for $\xi_0 = 3 \times 10^{-9}$ s cm⁻¹ and $x_0 = 3.08 \times 10^{21}$ cm = 1 kpc. The top panel shows a rapid decrease in $\rho(x)/\rho_0$ and $B(x)/B_0$ behind the front near $x = x_0$ as gas accelerates away from the front into the lobe. The decreasing field strength in this accelerating flow is responsible for the narrowness of the observed limb brightened region at the lobe boundary. As x approaches x_0 from the lobe side, the cosmic ray diffusion coefficient $\kappa(x)$ (really $\kappa_\perp(x)$) plummets (along with $P_c(x)$) toward zero. On the cluster gas side of the front, $x > x_0$, where e_c is assumed to vanish, equation (9) requires that the flow velocity u remains locally uniform, $u(x > x_0) = u(x_0)$ along with the gas density and pressure. In addition, the magnetic field perpendicular to the flow continues to be uniform in the cluster gas beyond the radio lobe; bright radio rims occur as the diffusing electrons encounter this inflowing field. Evidently the tangential B field just ahead of the front is prepared in a compression between a subsonically outwardly expanding lobe and/or radiatively cooling cluster gas inflowing toward the lobe.

2.3. X-ray Features Associated with Radio Lobes

The pressure of relativistic electrons responsible for the radio emission observed in Virgo is unlikely to be the only or even the dominant non-thermal pressure component. The electron energy distribution $EN(E)$ peaks toward lower energies that emit at radio wavelengths too large to be currently detected. In studies of radio synchrotron and inverse Compton X-ray emission from electrons of the same energy inside X-ray cavities, assumed to be in pressure balance with local cluster gas, Croston et al. (2005) find no evidence for an energetically dominant

relativistic proton population. Although relativistic protons dominate the cosmic ray energy density in the Milky Way, they are difficult to detect in extragalactic sources.

Observational efforts should be made to detect the total non-thermal pressure in the Virgo radio lobes by identifying a lower gas pressure in the lobe compared to that in cluster gas outside the lobes at the same distance from the cluster center. Small irregularities in the azimuthally-averaged radial X-ray surface brightness profile in Virgo have been discussed in detail (Churazov et al. 2008), but a similar effort should be made to detect azimuthal variations in the X-ray surface brightness and gas pressure that correlate with the radio lobe structures. Since the radio lobe boundaries are well-defined, it should be possible to detect or set rather tight limits on the contribution of non-thermal components to the pressure in the lobe.

To explore this possibility, we constructed an approximate azimuthally-averaged radial (bolometric) X-ray surface brightness profile in Virgo (using the Ghizzardi et al. 2004 observations) and estimated the brightness reduction produced by depleting the gas density by two inside symmetric radio lobes of radius 23 kpc with centers 13.7 kpc from the cluster center in M87, assumed to be in the plane of the sky. We found that the X-ray surface brightness in mid-lobe regions is depleted by about 0.55 - 0.70 along M87-centered circles of radius 25 - 30 kpc, circles that also contain large regions of cluster gas outside the lobes that can be used for calibration. Near the lobe rims the X-ray surface brightness profile is likely to have a slope change, not a sharp discontinuity. The gas temperature may also differ across the lobe boundary since thermal conductivity will also be reduced by magnetic fields tangent to the boundary.

However, no lowering of the gas pressure in the radio lobes is apparent in the recent Virgo pressure image of Million et al. (2010), although low amplitude thermal pressure variations may eventually be detected with dedicated X-ray observations. If the contribution of cosmic rays to the total pressure is lower than we assume here, $P_c/(P + P_c) \approx 1/3$, the condition (24) for radio limb brightening requires a larger value of the spectral index α . For example, if P_c contributes only about 13% of the total pressure in the lobes, we require $\alpha \gtrsim 3$ for limb-brightening, but the structure of the diffusion front remains similar to those in Figures 2, 4 and 5.

The terminology for feedback-related diffuse radio emitting regions in galaxy clusters includes mini-halos, lobes and emission from X-ray cavities. We stress here that all of these extended radio-emitting regions must to some extent also be X-ray cavities, although may not have been detected with current X-ray observations particularly if $P_c \ll P$. Another complication that can arise in detecting X-ray cavities is the possibility of inverse Compton X-ray emission from upscattered cosmic microwave radiation, as recently observed in the large radio lobes in the Fornax cluster (Tahiro et al. 2009; Seta et al. 2011). Additional inverse Compton X-radiation that accompanies the radio emission would make detection of thermal cavities in the hot cluster gas more difficult.

3. FINAL REMARKS

Our simple calculation shows that cosmic rays in the Virgo cluster can be strongly confined within certain re-

gions of the cluster gas. Confinement is aided by magnetic fields that are tangent to the boundaries of these regions where the synchrotron emission decreases with decreasing cosmic ray diffusivity. Broad gaussian-shaped diffusion fronts associated with free diffusion at constant diffusivity κ in the cluster gas are not present in Virgo and cannot be generally assumed. Nevertheless, free diffusion of synchrotron emitting electrons may occur in nature and can be detected by spectral *flattening* near the outer edges of gaussian-broadened radio lobes because the diffusion coefficient increases for more energetic relativistic electrons.

The radio lobes in Virgo, and those in other clusters, are naturally buoyant because the additional partial pressure of cosmic rays depresses the thermal gas pressure (and gas density) in the lobe to match the cluster gas pressure just outside the lobe. As these large buoyant lobes attempt to slowly rise in the cluster atmosphere, they encounter cluster gas that is slowly inflowing due to radiation losses, compressing gas throughout the lobes and at the lobe-cluster gas boundaries. This compression forces the cluster magnetic field to become nearly perpendicular to the direction of compression, and tangent to the diffusion front interface, sharply limiting cosmic ray diffusion in this direction. In this sense the propagation of cosmic rays in cluster gas is self-limiting.

Except for the idealized singular case where the magnetic field is aligned precisely perpendicular to the diffusion front, as the expanding radio lobe and inflowing cluster gas mutually compress at glacial velocities, the magnetic field is forced to become tangent to the lobe boundary, becoming locally perpendicular to the compression regardless of its initial morphology. Evidently, a similar field-orienting compression occurs throughout the Virgo radio lobes, as supported by the polarization vectors in Figure 3. Such an alignment cannot simply be due to so-called “draping” of magnetic lines of force along its boundary since it is most unlikely that large scale magnetic field lines exist that connect across the lobe boundaries and throughout the interior of the lobes. Considering the dynamic activity inside the lobes visible in Figure 1, the spatial continuity of polarization vectors in Figure 3 from one observed beam position to the next along the field direction almost certainly does not trace a single magnetic line of force. Instead, we envision a field that naturally aligns perpendicular to a large scale one-dimensional compression much like spaghetti arranged itself horizontally when served on a dinner plate. Magnetic fields *of all spatial scales* are aligned in this manner, accounting for the remarkable consistency of the direction and magnitude of the polarization vectors observed in Virgo. The insensitivity of compressive field alignment to the spatial scale or local curvature of the field is particularly relevant to galaxy clusters like Virgo where the relativistic electron gyroradius $r_g = \gamma mc^2/eB = 5 \times 10^{12}(\gamma/10^4)(B/3\mu\text{G})^{-1}$ cm is 10^{10} times smaller than the radius of the lobes. The polarizing magnetic field experienced by synchrotron-radiating electrons, when averaged over kpc-sized radio beams as in Figure 3, gives the impression of magnetic field lines that are coherent over kpc-scales, i.e. that single field lines are “draped”. However, the field seen by the radiating electrons is likely to have a range of different scales (radius of curvature) but the electrons responsible for the

observed polarized emission radiate from field segments that are locally aligned perpendicular to both the line of sight and to the large scale compression. The radiating segments do not need to be (and are probably not) connected along a single large scale line of force.

The region of compressionally aligned B in our diffusion fronts could extend significantly beyond the lobe boundary where $j_\nu \rightarrow 0$ in Figure 1. A similar cosmic ray confinement by boundary-tangent \mathbf{B} is also expected in X-ray cavities with corresponding radio continuum limb-brightening and high polarization near the radio emission boundaries at the cavity walls. Detailed radio observations of magnetic field polarization and alignment along the walls of known X-ray cavities do not appear to have been attempted.

Our steady state solutions describe the upstream diffusion of relativistic cosmic rays from a radio lobe slowly compressing against cluster gas where the cosmic ray energy density is negligible. As indicated by radio polarization observations of Virgo, the magnetic field in the upstream cluster gas is aligned largely tangent to the lobe boundary and perpendicular to the gas flow. At the leading edge of the advancing cosmic ray diffusion front, where non-thermal particles first penetrate into the undisturbed cluster gas, the diffusion coefficient declines sharply with increasing magnetic field strength and its unfavorable alignment. Nevertheless, the small non-thermal pressure introduced by diffusing cosmic rays near the leading edge of the front lowers the local gas pressure and the reduced gas density $\rho = P/c_s^2$ drives a gas flow that expands back toward the radio lobe in a direction opposite to the forward advancing diffusion. Under certain conditions bright radio synchrotron rims are expected along the diffusion front at the lobe boundary as shown in Figure 1. As the steady diffusion front is approached from the radio lobe side, the synchrotron

emissivity rises because of the increasing magnetic field ($B \propto \rho$) but ultimately declines with the decreasing number density of synchrotron-emitting electrons. The sharpness of the radio synchrotron emission peaks and its decline to zero flux depends on the rate that the diffusion coefficient decreases across the diffusion front. Bright radio synchrotron rims are expected when the partial pressure of cosmic rays inside the radio lobe and the spectral index are sufficiently large.

Our analysis in this paper describes lobe rim profiles that are in qualitative agreement with the radio image of Virgo. As more data become available at several radio frequencies, a precise fit to the radio limb brightening at the lobe boundaries in Virgo may allow for the first time an estimate of the spatial profiles of the field strength $B(x)$ and the corresponding cosmic ray diffusion coefficient $\kappa(x)$. In addition, it may be possible to determine from X-ray observations whether the total non-thermal pressure in the Virgo lobes can be estimated from azimuthal gas density and pressure variations across the lobes along cluster-centered circular arcs that intersect both the radio lobes and cluster gas outside the lobes. Indirect detection or non-detection of the pressure of additional unobserved thermal or relativistic particles in radio lobes would have broad astrophysical implications. Finally, we note that the presence of a gas density jump at the lobe-cluster gas transition in Virgo as in Figure 5 may help to divert and divide the outflowing gas at the top of the eastern mushroom-like flow visible in Figure 1.

We thank Fill Humphrey for discussions about azimuthal variations in the X-ray emission from Virgo. Studies of the evolution of hot gas in elliptical galaxies at UC Santa Cruz are supported by NSF and NASA grants for which we are very grateful.

REFERENCES

- Bonafede, A., Feretti, L., Murgia, M., Govoni, F., Giovannini, G., Dallacasa, D., Dolag, K., Taylor, G. B., 2010, *A&A*, 513, 30
 Churazov, E., Forman, W., Vikhlinin, A., Tremaine, S., Gerhard, O. & Jones, C., 2008, *MNRAS*, 388, 1062
 Croston, J. H., Hardcastle, M. J., Harris, D. E., Belsole, E., Birkinshaw, M., Worrall, D. M., 2005, *ApJ*, 626, 733
 Forman, W.; Nulsen, P.; Heinz, S.; Owen, F.; Eilek, J.; Vikhlinin, A.; Markevitch, M.; Kraft, R.; Churazov, E.; Jones, C., 2005, *ApJ*, 635, 894
 Ghizzardi, S., Molendi, S., Pizzolato, F., & De Grandi, S. 2004, *ApJ*, 609, 638
 Govoni, F., Feretti, L., 2004, *International Journal of Mod. Physics D13*, 1549
 Owen, Frazer N.; Eilek, Jean A.; Kassim, Namir E., 2000, *ApJ*, 543, 611
 Longair, M. S., 1994, in “High Energy Astrophysics”, vol 2, 2nd ed., (Cambridge University Press: Cambridge), p. 251
 Mathews, W. G. & Brighenti, F. 2008b, *ApJ*, 685, 128
 Mathews, W. G. & Brighenti, F. 2008a, *ApJ*, 676, 880
 Million, E. T., Werner, N., Simionescu, A., Allen, S. W., Nulsen, P. E. J., Fabian, A. C., Bohringer, H., & Sanders, J. S., 2010, *MNRAS*, 407, 2046
 Rottmann, H.; Mack, K.-H.; Klein, U.; Wielebinski, R., 1996, *A&A*, 309, L19
 Seta, H., Tashiro, M. S., Isobe, N. 2011, *Proceedings IAU Symposium No. 275, Jets on all Scales*, eds. G. E. Romero, R. A. Sunyaev & T. Belloni, p. 184
 Sturrock, P. A. 1994, in “Plasma physics: an introduction to the theory of astrophysical, geophysical & laboratory plasmas”, (Cambridge University Press: Cambridge), p. 40
 Tashiro, M. S., Isobe, N., Seta, H., Matsuta, K., & Yaji, Y. 2009, *PASJ*, 61, S327
 Werner, N. et al. 2010, *MNRAS*, 407, 2063
 Young, A. J.; Wilson, A. S.; Mundell, C. G., 2002, *ApJ*, 579, 560

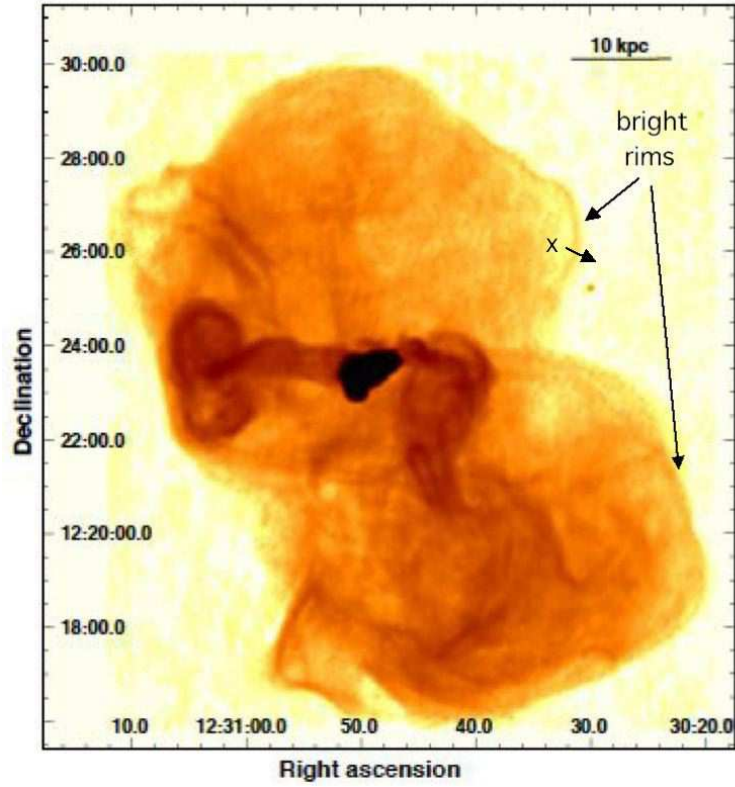


FIG. 1.— VLA radio image of Virgo at 90 cm (Owen, Eilek, Kassim 2000) showing radio continuum limb-brightening (beam resolution is 0.6 kpc). The small arrow at the western rim of the northern lobe shows the direction of increasing x in the diffusion front.

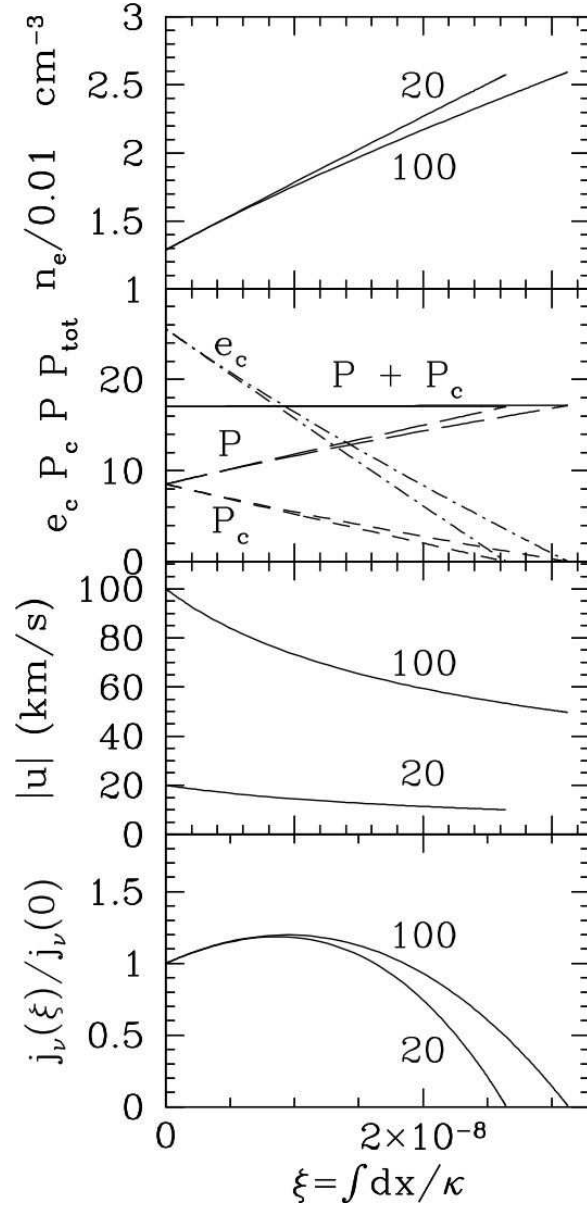


FIG. 2.— Two solutions of equations (15) with $u_0 = -20$ and -100 km s^{-1} , both with $T = 2.5 \times 10^7 \text{ K}$, $\rho_0 = 2.5 \times 10^{-26} \text{ gm cm}^{-3}$ (or $n_{e,0} = 0.0129 \text{ cm}^{-3}$), $(P_c/P)_0 = 1$, and $\phi_0 = -0.01$. The second panel from the top shows solutions for $e_c(\xi)$ (dashed-dot lines), $P_c(\xi)$ (short dashed lines), $P(\xi)$ (long dashed lines) and $P_t = P + P_c$ (solid lines). Solutions for $u_0 = -100$ extend to slightly larger ξ than those for $u_0 = -20 \text{ km s}^{-1}$. Bottom panel is the profile $j_\nu(\xi)$ of the radio synchrotron emissivity normalized to unity at $\xi = 0$ and with $\beta = 2$.

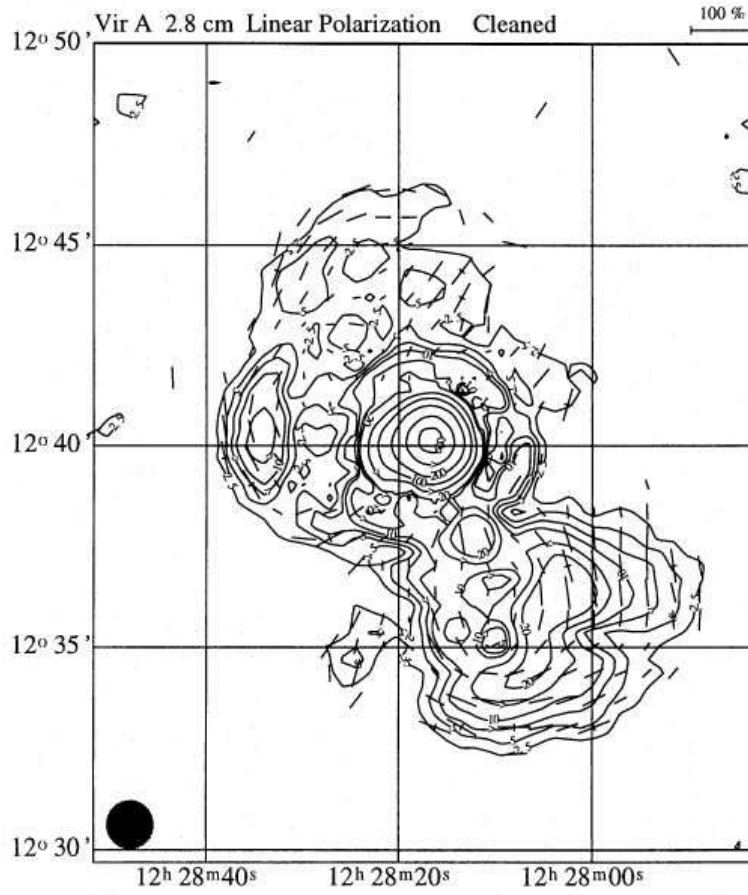


FIG. 3.— Polarized intensity map of Virgo at 2.8 cm with superimposed B vector with lengths proportional to the degree of linear polarization. Circle at lower left shows beam size (Rottmann, et al. 1996).

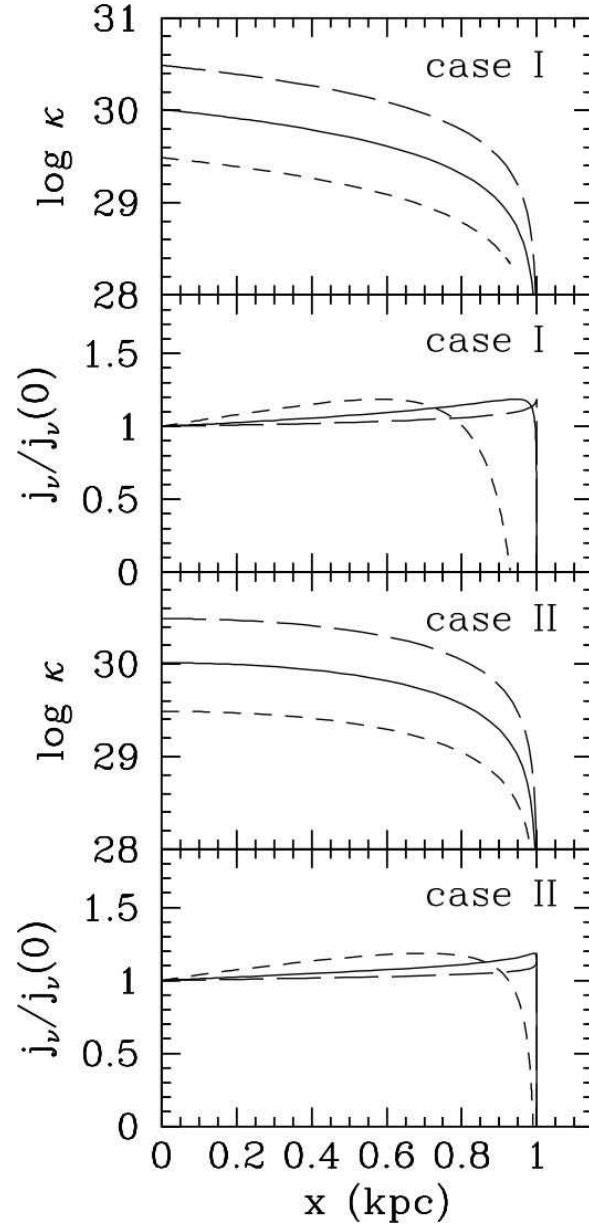


FIG. 4.— Normalized radio synchrotron emissivity profiles $j_\nu(x)/j_\nu(0)$ for the $u_0 = -20 \text{ km s}^{-1}$ flow in physical space for Case I and II diffusion coefficients $\kappa(x)$ ($\text{cm}^2 \text{ s}^{-1}$) both with $x_0 = 1 \text{ kpc}$. The three profiles in each panel correspond to $\xi_0 = 1 \times 10^{-9}$ (long dashed line), $\xi_0 = 3 \times 10^{-9}$ (solid line), and $\xi_0 = 1 \times 10^{-8}$ (short dashed line), all in units of s cm^{-1} .

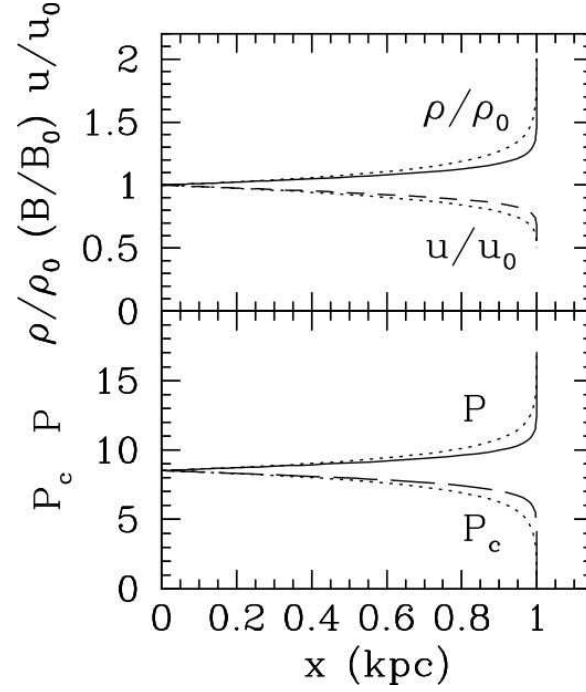


FIG. 5.— Diffusion front profiles for $u_0 = -20 \text{ km s}^{-1}$ flow with $\xi_0 = 3 \times 10^{-9}$ and $x_0 = 1 \text{ kpc}$. Coordinate transformations $x(\xi)$ for Case II are shown in solid and long dashed curves; adjacent dotted lines show profiles for Case I. *Upper panel:* Gas density and magnetic field profiles (solid line) and flow velocity (short dashed line), all normalized to values at $x = 0$. *Lower panel:* gas pressure $P(x)$ (solid line) and cosmic ray pressure $P_c(x)$ (long dashed line) both in units of $10^{-11} \text{ dy cm}^{-2}$.